Optik - International Journal for Light and Electron Optics 181 (2019) 1000–1012

Contents lists available at ScienceDirect

Optik

journal homepage: www.elsevier.com/locate/ijleo

Original research article

A hybrid control strategy for the optoelectronic stabilized platform of a seeker

Mingyue Zhang[a,*], Hui Liu[a], Hongwei Zhang[a], Xikui Miao[b]

[a] Changchun Institute of Optics, Fine Mechanics and Physics, Chinese Academy of Sciences, No.3888, Dongnanhu Rd., Changchun, 130033, China
[b] Luoyang Electronic Equipment Test Center of China, Key Laboratory of Electro-Optical Countermeasures Test & Evaluation Technology, Luoyang, 471000, China

ARTICLE INFO

Keywords:
Optoelectronic stabilized platform of a seeker
Butterworth low pass filter
Disturbance rejection rate of a seeker
Disturbance observer
Notch filter
Incomplete derivative proportional integral derivative (IDPID) controller

ABSTRACT

In order to improve the rapidity and disturbance rejection rate of the optoelectronic stabilized platform of a seeker, a hybrid control strategy for stabilized loop of the optoelectronic stabilized platform is proposed in this paper. The hybrid control strategy consists of Butterworth low pass filter, disturbance observer (DOB), notch filter and incomplete derivative proportional integral derivative (IDPID) controller. Firstly, the controlling architecture and stabilized principle of the optoelectronic stabilized platform are analyzed. Secondly, the hybrid control strategy is analyzed. Finally, experiments of the seeker using the proposed hybrid control strategy and traditional proportional integral (PI) controller are carried out. In addition, the experimental set-up provides a comparison to the two controllers. Experimental results show that the requirements are totally met, the bandwidth of the stabilized loop with the proposed hybrid control strategy is 133.6 rad/s, and the disturbance rejection rate is 2.45%, which improve the performance of the seeker effectively.

1. Introduction

The semi-active laser seeker is a widely used guidance mode in the guidance weapons developing process. The principle of the semi-active laser seeker (Fig. 1) is that a laser designator which could be assembled on the warplane or the missile truck apart from missile is used to irradiate a target, and then, a laser spot signal reflected from the target is received by a laser detector on the optoelectronic stabilized platform of the seeker [1]. The laser detector acquires the information of the reflected laser and transmits such information to the data process system to obtain the line-of-sight (LOS) which is the command of the optoelectronic stabilized platform of the seeker. The optoelectronic stabilized platform of the seeker maintains stabilizing the LOS axis when suffering inner and external disturbances of the missile. With this technique, the laser is kept pointing to the target, and the missile is launched or dropped somewhere near the target. When the distance between the missile and the target becomes close enough, the laser seeker detects the target and adjusts the projectile trajectory towards the target, which achieves the precision strike. As a result, the optoelectronic stabilized platform of seeker plays an important role in the seeker. The performance of the optoelectronic stabilized platform affects the performance of missiles. With the urgent demand of the precision-guided missiles, it is necessary to improve the performance of the optoelectronic stabilized platform of the seeker. The optoelectronic stabilized platform of the seeker is structured by two-axis inertial stabilized platform. The rapidity and disturbance rejection rate of the inertial stabilized platform are two

* Corresponding author.
E-mail addresses: zyy_2011@163.com (M. Zhang), liuh6009@163.com (H. Liu), zhanghw135@163.com (H. Zhang), miaoxikui@163.com (X. Miao).

https://doi.org/10.1016/j.ijleo.2018.12.168
Received 16 December 2018; Accepted 29 December 2018

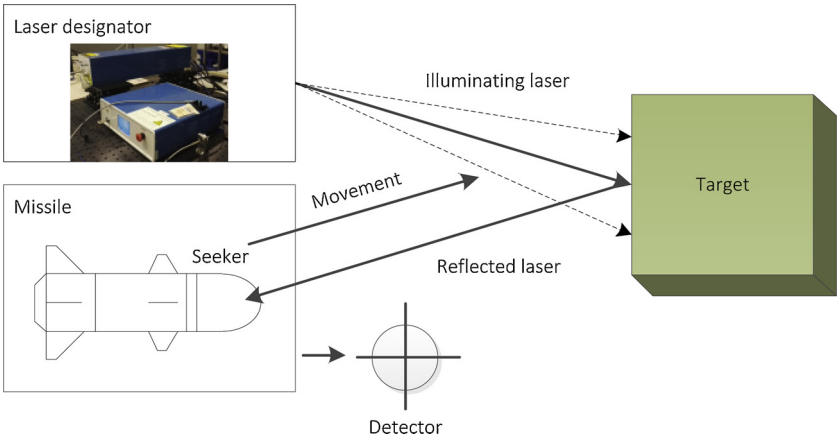

Fig. 1. The principle of semi-active laser guidance.

important indexes. The control strategy of the inertial stabilized platform determines the indexes of the system. However, owing to the complex interaction between the mechanical design, and the dynamics of the system and sensor systems, the controller design poses a challenging problem. To stabilize the platform of the seeker precisely, it is significantly important to design an effective control strategy for suppressing the disturbance. The pointing control is implemented by three servo loops, current loop, rate loop or stabilized loop and position loop or tracking loop. The current loop is carried out by combining with integration driver amplifier, which serves to restrain the torque disturbance. The stabilized loop aims to isolate the disturbances of the system and assures the rapidity of the system [2]. The tracking loop aims to track the LOS kinematics. Consequently, there is a lot of work to do for the controller design of stabilized loop of the stabilized platform.

Because traditional proportional integral derivative (PID) controller has conflicts between dynamics performance and noise, it cannot eliminate the subsistent time-varying disturbances. During the past decades, a number of control strategies have been used for two-axis gimbal stabilized platform, including H ∞ control [3],internal mode control [4], fuzzy control [5], sliding mode control (SMC) [6], neural networks control [7], active disturbance rejection control (ADRC) [8]. Although the proposed control strategies have improved the performance of the stabilized platform, they have the disadvantage of model complexity and it is difficult to carry out in actual utility. So we adopted incomplete derivative proportional integral derivative (IDPID) controller, which takes full advantage of the PID controller and also has the advantage of reducing conflicts between dynamics performance and noise.

As we know, a more reliable method for reducing the disturbance is to develop disturbance estimation and compensation [9]. The observers are adopted including sliding mode observer (SMO) [10], extended state observer (ESO) [11], finite-time disturbance [12], disturbance observer (DOB) and so on. Among all the observers, DOB originally proposed by Ohnishi [13] has been utilized in various specific conditions. It can effectively observe the disturbance and generate appropriate compensation signals to the system [14]. The equivalent structure which is proposed by C.*J*. Kempf is widely used in various applications [15,16]. DOB has the virtue of simple structure, small amount of calculation and effective suppression of external disturbances [17]. The disadvantage of the design of DOB is that it needs the inverse of the system. Considering that triple control loops in the system, the model of the stabilized loop can be easily obtained by model identification, so this problem can be solved easily in this paper. In addition, the precision of the gyro is not satisfied the demand of the stabilized platform, it is necessary to design a filter to reduce the noise. As a result, Butterworth low filter is utilized in this paper. Considering the integrity and particularity of the system, since there is a similar resonant frequency in the frequency characteristics curve, notch filter is adopted to eliminate it.

In this paper, in order to improve the rapidity and disturbance rejection rate of the optoelectronic stabilized platform of a seeker, a hybrid control strategy consists of Butterworth low pass filter, DOB, notch filter and IDPID controller for the stabilized loop of the optoelectronic stabilized platform is proposed. The outline of this exposition is as follows. The optoelectronic stabilized platform of seeker is analyzed and models for the kinematics and dynamics are illustrated in Section 2. The control strategy is proposed for the optoelectronic stabilized platform of seeker in Section 3. Experiments results are given to analyze the specific features of the proposed strategy in Section 4. Moreover, the effectiveness is compared with traditional PI controller. Finally, conclusions are presented in Section 5.

2. Modeling of the optoelectronic stabilized platform of the seeker

Fig. 2 displays the schematic diagram of the seeker, which consists of the dome, optics system, four-quadrant detector, the optoelectronic stabilized platform, printed-circuit-board (PCB). In particular, optics system is used to deal with the laser, and four-quadrant detector is used to receive the laser information and completes the transmission of the laser to voltage information. The optoelectronic stabilized platform consists of pitch gimbal, yaw gimbal, sensors and motors. Pitch gimbal is used to fit the optics system. Yaw gimbal is the outer gimbal of the optoelectronic stabilized platform, which is mounted on the missile. Angular velocities of the two gimbals are measured by micro-electro-mechanical system (MEMS) gyro that is mounted on the pitch gimbal. Thus, it

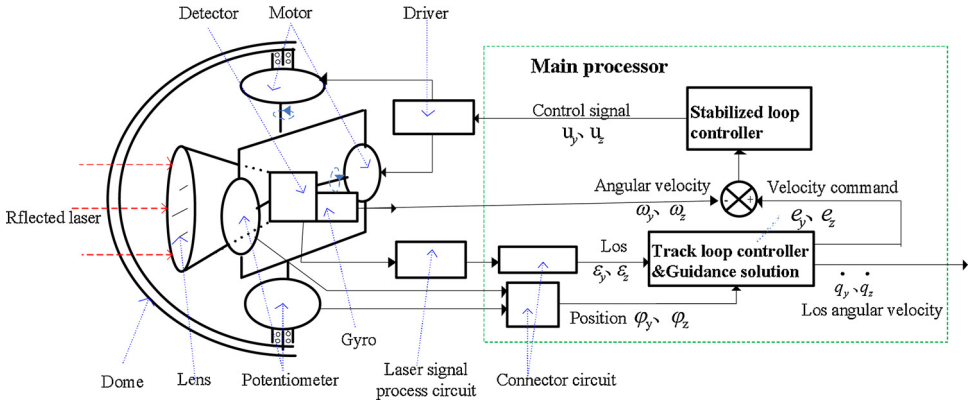

Fig. 2. Schematic diagram of the seeker.

demonstrates that the system adopts the direct stabilization strategy [18]. The position of the gimbal is measured by the potentiometer. Torque motors are applied as the direct drive devices. PCB is used to process the signal and realize controller.

The sketch of the missile in Fig. 3 demonstrates that the platform comprises reference frames that are pitch gimbal frame o-$x_2y_2z_2$, yaw gimbal frame o-$x_1y_1z_1$ and the base frame o-$x_0y_0z_0$ (missile). The coordinate transformation between the base coordinate frame and the yaw coordinate frame is as follows

$$R_{0,1}(0) = \begin{bmatrix} \cos\theta_1 & 0 & -\sin\theta_1 \\ 0 & 1 & 0 \\ \sin\theta_1 & 0 & \cos\theta_1 \end{bmatrix}^{-1} \tag{1}$$

Where$\theta_1$is the relative azimuth angular between the yaw coordinate frame and the base coordinate frame.

The rate vector of the yaw gimbal $\omega_1$related to the rate vector of the base coordinate frame $\omega_0$can be derived by

$$\omega_1 = R_{0,1}^{-1}\omega_0 + \begin{bmatrix} 0 \\ \dot{\theta}_1 \\ 0 \end{bmatrix} = \begin{bmatrix} \cos\theta_1 & 0 & -\sin\theta_1 \\ 0 & 1 & 0 \\ \sin\theta_1 & 0 & \cos\theta_1 \end{bmatrix} \begin{bmatrix} \omega_{0x} \\ \omega_{0y} \\ \omega_{0z} \end{bmatrix} + \begin{bmatrix} 0 \\ \dot{\theta}_1 \\ 0 \end{bmatrix} \tag{2}$$

Likewise, the coordinate transformation between yaw coordinate frame and pitch coordinate frame is as follows

$$R_{1,2}(0) = \begin{bmatrix} \cos\theta_2 & \sin\theta_2 & 0 \\ -\sin\theta_2 & \cos\theta_2 & 0 \\ 0 & 0 & 1 \end{bmatrix}^{-1} \tag{3}$$

Where$\theta_2$is the relative elevation angular between the pitch coordinate frame and the yaw coordinate frame.

The rate vector of the pitch gimbal$\omega_2$related to the rate vector of the yaw gimbal$\omega_1$is as follows

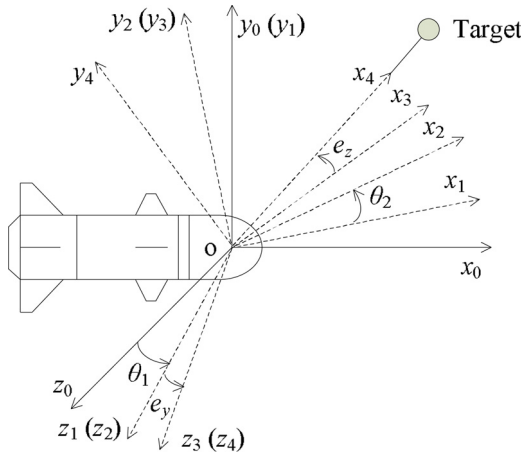

Fig. 3. Sketch of the missile.

$$\omega_2 = R_{1,2}^{-1}\omega_1 + \begin{bmatrix} 0 \\ 0 \\ \dot{\theta}_2 \end{bmatrix} = \begin{bmatrix} \cos\theta_2 & \sin\theta_2 & 0 \\ -\sin\theta_2 & \cos\theta_2 & 0 \\ 0 & 0 & 1 \end{bmatrix} \begin{bmatrix} \omega_{1x} \\ \omega_{1y} \\ \omega_{1z} \end{bmatrix} + \begin{bmatrix} 0 \\ 0 \\ \dot{\theta}_2 \end{bmatrix} \tag{4}$$

Substituting Eq. (2) into Eq. (4), the rate vector of the pitch coordinate frame$\omega_2$is related to the base coordinate frame rate vector$\omega_0$by

$$\omega_2 = \begin{bmatrix} \omega_{0y}\sin\theta_2 + \dot{\theta}_1\sin\theta_2 + \omega_{0x}\cos\theta_1\cos\theta_2 - \omega_{0z}\sin\theta_1\cos\theta_2 \\ \omega_{0y}\cos\theta_2 + \dot{\theta}_1\cos\theta_2 - \omega_{0x}\cos\theta_1\sin\theta_2 + \omega_{0z}\sin\theta_1\cos\theta_2 \\ \omega_{0x}\sin\theta_1 + \omega_{0z}\cos\theta_1 + \dot{\theta}_2 \end{bmatrix} \tag{5}$$

In order to stabilize the LOS, let$\omega_{1y} = 0$, $\omega_2 z = 0$. Because the gyro is fitted on the pitch gimbal, we can get the Eq. (6) from Eq. (2) and Eq. (5) as follows

$$\begin{cases} \omega_{1y} = \omega_{0y} + \dot{\theta}_1 = \frac{\omega_{gyro\_y}}{\cos(\theta_2)} + \omega_{1x}\tan(\theta_1) \\ \omega_2 z = \omega_{gyro\_z} \end{cases} \tag{6}$$

The gimbal dynamics model can be derived from the torque relationships about the yaw gimbal, pitch gimbal and base axis based on rigid body dynamics [2]. In order to simplify the analysis, cross-coupling torque between the yaw gimbal and pitch gimbal is regarded as disturbances.

The dynamics of elevation axis can be expressed in terms of the base inputs as

$$T_{ez} = J_{2z}\omega_{2z} + \tau_{pf} + T_{pd} \tag{7}$$

Where J_{2p} is the inertia of the$z$axis of pitch gimbal, $T_{ez}$is the control motor torque of pitch gimbal, $\tau_{pf}$is the linear friction torque, $T_{pd}$is the disturbance such as nonlinear cable restraint torque, nonlinear friction torque, cross-coupling torque from yaw gimbal and external disturbance.

In a similar manner, the azimuth axis dynamics of the can be then expressed in terms of the base inputs as

$$T_{ay} = J_{1y}\omega_{1y} + \tau_{yf} + T_{yd} \tag{8}$$

Where$J_{1y}$is the inertia of the$y$axis of yaw gimbal, $T_{ay}$is the control motor torque of pitch gimbal, $\tau_{yf}$is the linear friction torque, $T_{yd}$is the disturbance such as nonlinear cable restraint torque, nonlinear friction torque, cross-coupling torque from pitch gimbal and external disturbance.

3. Controller design

The control strategy of the yaw and pitch gimbal is the same except that the yaw frame needs secant compensation. In this paper, yaw gimbal is used as the research object. The overall control strategy of the platform is composed of three hierarchical layers. The inner-loop controller is developed by hardware. The design of the current loop is combined with motor driver amplifier and the specific type of the driver amplifier is MSK4253. The final bandwidth of the current loop is adjusted by configuring the driver chip. The middle loop is implemented by the proposed hybrid controller. P controller is utilized to control the outer-loop, which avoids having to control loops that both have integral parts in cascade (as they might counteract each other). The block diagram of the three-loop controller is illustrated in Fig. 4. It can be observed that the stabilized loop design of the platform is the key for improving the dynamic response and the disturbance rejection rate. The proposed design procedure of the controller strategy can be summarized in the flow chart (Fig. 5).

3.1. Butterworth filters

Owing to the characteristics of simplicity and acceptable performance, Butterworth filters are commonly used to remove high

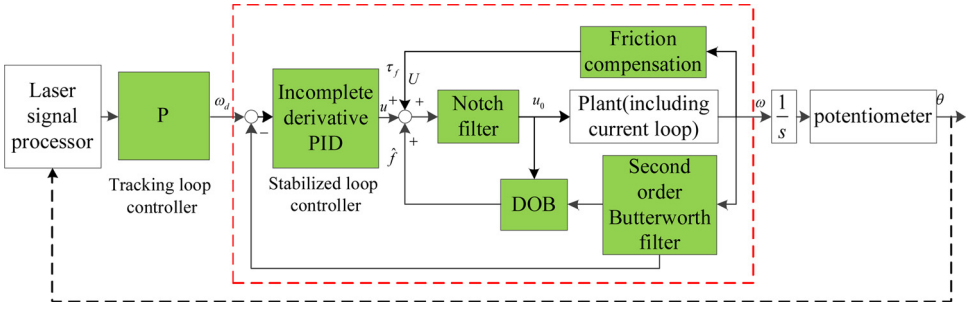

Fig. 4. Control framework of the optoelectronic stabilized platform of the seeker.

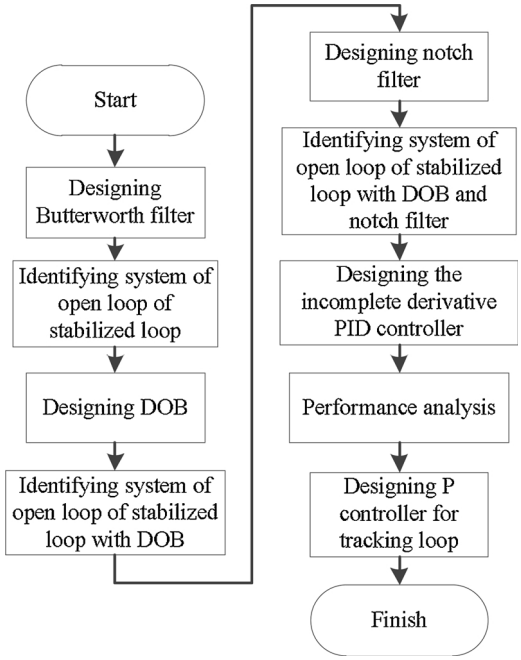

Fig. 5. Flowchart of the proposed controller strategy.

frequency noise in gyro filtering. A low-pass Butterworth filter of second order has a transfer function as follows

$$H(s) = \frac{1}{(\frac{s}{2\pi\omega_c})^2 + 1.414(\frac{s}{2\pi\omega_c}) + 1} \tag{9}$$

Where$\omega_c$is the cut-off frequency which is the only parameter set by user [19,20]. The selection of the cut-off frequency is important in the operation of the filter. Generally, the cut-off frequency takes values of over five times of the bandwidth of the closed loop, which denotes the suitable frequency values to be used in the filtering process. When the cut- off frequency and the filter order are specified, the poles and the transfer function of the filter can easily be obtained. In this paper, a cut-off frequency is selected as 100 Hz, since the bandwidth of the stabilized closed loop is approximately 18 Hz.

3.2. Disturbance observer

DOB is used for rejecting internal and external disturbances acting on the plant. The key point of DOB is to use measurements of the plant input and output to reconstruct the disturbance. The block diagram of the equivalent DOB based scheme is illustrated in Fig. 6. Where$G$(s)is the real controlled plant, G_n(s)is the nominal model of G(s), $u_i$is the input of the system, d, ξ, y denote the disturbance of the system, measurement noise, and system output respectively which is used to compensation for the disturbance, Q(s) is the low pass filter of DOB.

The transfer function between$u_i$and$y$can be expressed as follows

$$Gu_iy = \frac{G(s)G_n(s)}{G_n(s) + [G(s) - G_n(s)]Q(s)} \tag{10}$$

$$Q(s) = \frac{\sum_{k=0}^{M} \alpha_k(\tau s)^k}{(\tau s + 1)^N} \tag{11}$$

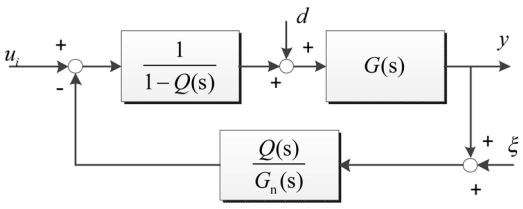

Fig. 6. Block diagram of the equivalent DOB-based control scheme.

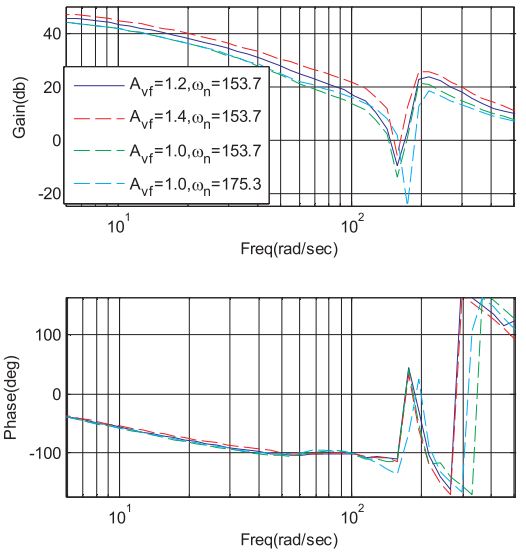

Fig. 7. Bode diagrams of the system considering different value of A_{vf} and ω_n.

When assuming ideal disturbance compensation, the effects of disturbances are entirely compensated. Because$G(s)$is the system including current loop, which can be approximately, regarded as a second order system. So the selection of $G_n(s)$is obtained by the identification of the system. And then, the determination of $Q(s)$is followed the principle proposed by H.S. Lee [21].

3.3. Notch filter

Nonlinear factor and mechanical design in the stabilized platform will cause resonance of the system to shift towards frequency that affects the stability of the system. Notch filter is widely used in servo systems for suppressing a resonance that is a major obstacle to improve their performance. A notch filter is a linear time-invariant system with a magnitude response that vanishes at a particular point on the imaginary axis, which is called as the notch frequency. In this paper, the notch frequency can be obtained by identification of the frequency characteristic curve of the closed loop system. The order and coefficients of the notch filter are empirically determined. As a result, the second-order notch filter is used in this paper and the typical transfer function is as follows

$$A(s) = \frac{A_{vf}(1 + (\frac{s}{\omega_n})^2)}{1 + 2(2 - A_{vf})\frac{s}{\omega_n} + (\frac{s}{\omega_n})^2} \tag{12}$$

where $A_{vf}$is a pole radius controlling the notch bandwidth (notch depth), $\omega_n$is the notch frequency which is determined by the resonant point. To compare$A_{vf}$and$\omega_n$thoroughly, the Bode diagrams of the system with notch filter by different A_{vf}andω_n are shown in Fig. 7. It can be seen from Fig. 7 that the bandwidth of the system depends on the gainA_{vf}andω_n. The resonant frequency of the system determined the notch frequency. Compared to the system that has time-varying sinusoidal interference components, the system in this paper has a fixed center frequency of narrow-band interference components. As a matter of fact, $A_{vf}$is always determined by trial and error, in this paper, $A_{vf} = 1$.

3.4. Incomplete derivative PID controller

A PID controller is the most widely used controllers in many fields because of ease design and low cost implementation. The typical controller of stabilized loop is designed with PID as follows

$$G_c(s) = k_p + k_d s + \frac{k_i}{s} \tag{13}$$

where k_p, k_i, k_d are the corresponding coefficients of the PID controller. The proportional gain $k_p$is used for anticipation of error, the integral gain $k_i$determines the reactive action to sum of errors, and derivative gain$k_d$determines the action based on the rate of change of error. The model of the power amplifier can be denoted by 1.

IDPID controller is used in this paper, and the equation of the controller is as follows

$$G_c(s) = [k_p + k_i(\frac{1}{s}) + k_d(\frac{Ns}{s + N})] \tag{14}$$

The characteristic of the controller is that the controller adds a low pass filter $G_f(s) = \frac{N}{s+N}$to improve the performance of the system.

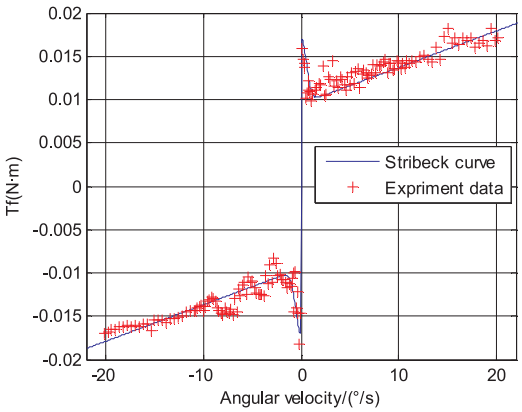

Fig. 8. Stribeck model identification curve of the stabilized platform.

Friction compensation is added to this control strategy, and the Stribeck friction model based on the stabilized platform is as follows

$$T_f = \begin{cases} T_f(\dot{\theta}) & \dot{\theta} \neq 0 \\ T_c & \dot{\theta} = 0 \quad |T_c| < T_s \\ T_s \operatorname{sgn}(T_c) & \dot{\theta} = 0 \quad T_s \leq |T_c| \end{cases} \tag{15}$$

where $T_f(\dot{\theta}) = [T_c + (T_s - T_c)e^{-(\frac{\dot{\theta}}{\dot{\theta}_s})^{\alpha}}]\operatorname{sgn}(\dot{\theta}) + k_v\dot{\theta}$, T_f is the total friction torque, T_c is the coulomb friction torque, T_s is the static friction force, k_v is the viscous friction coefficient, respectively, $\dot{\theta}_s$is the velocity of Stribeck model, and $\alpha$is an empirical parameter, here $\alpha = 2$. Using the least square method, static parameters are obtained from Stribeck model identification curve.

Friction parameters are identified off-line when the stabilized platform works at constant speed. Based on identified parameters, linear compensator is designed to compensate the friction disturbance in the stabilized loop. Stribeck model identification curve of stabilized platform is shown in Fig. 8 and identification parameters of Stribeck model is shown in Table 1.

4. Experiments and results

4.1. Experimental setup

From Sections 2 and 3, the principle of the controller strategy is given. In order to validate the effectiveness of the proposed control scheme for the platform, some experiments are carried out in this section. In this section, a typical pitch gimbal is used to clarify the hybrid controller deriving procedures and illustrate the effectiveness of the proposed hybrid controller. Fig. 9 depicts the setup used in the experiments. It consists of the stabilized platform of a seeker, personal computer, industrial computer with a data acquisition card, and driver. The Xpc real time system is utilized to generate the control input of the stabilized platform. Industrial computer with a data acquisition card acquires data from gyro and potentiometer. The sampling time of the stabilized loop is 1 ms. The sampling time of the tracking loop is 50 ms. Bilinear transform between $s$and z domains is utilized to discrete the algorithm proposed above.

The goal is to control the stabilized loop of the stabilized platform meet the demand that a bandwidth is above 15 Hz, the disturbance rejection rate under 1°3.5 Hz input is less than 5%, and the static error of the gyro output is less than 0.25°/s. The design of the proposed controller strategy is summarized in the flowchart in Fig. 5. There are nine steps for controller design process: designing Butterworth filter, identifying system of open loop of stabilized loop, designing DOB, identifying system of open loop of stabilized loop with DOB, designing notch filter, identifying system of open loop of stabilized loop with DOB and notch filter, designing the incomplete derivative PID controller, performance analysis, and designing P controller for tracking loop. The main steps of controller design are given in Section 4.2.

Table 1
Identification parameters of Stribeck model.

Parameters	T_c /(N m)	T_s /(N m)	$\dot{\theta}_s$/(°/s)	k_v
Values	0.0095	0.017	15.2	2.1×10^{-5}

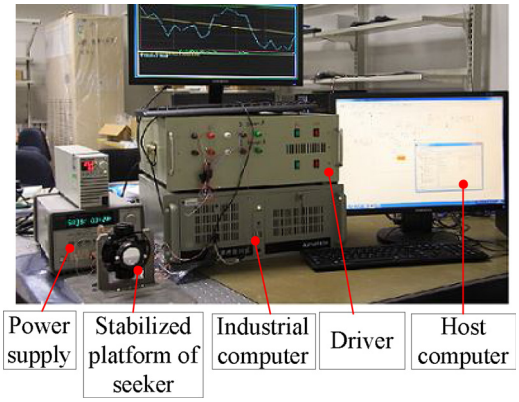

Fig. 9. Experimental setup of the stabilized platform.

4.2. Controller implemented and performances verification on the stabilized platform

The current loop is implemented by configuring the driver chip and the bandwidth of the current loop is 1300 Hz. According to the theory of Section 3.1, Butterworth filter of a second order, low-pass filter with cut-off frequency 100 Hz by trial and error is used to remove the main noise. The outputs of the gyro with filter and without filter are shown in Fig. 10. The static error of gyro output with filter is less than 0.25°/s which satisfies the demand of the system. The filter effectively improves the noise components, with attenuation greater than 30%. Both the traditional PI controller and the hybrid controller are implemented on the platform.

An identification algorithm for the system based on correlation analysis method is used in this paper. Some possible signals such as filtered Gaussian white noise, multi-sinusoidal signals, and pseudo-random binary signals [22] are always used as the input signals of the correlation analysis method. Here, we use pseudo-random white noise as the input signal. The theory of the identification can refer to [23,24].The range of random white noise is from −0.3 to 0.3. We record the output of the system and deal with the input and output. The least-mean-square (LMS) algorithm is used, since it is relatively simple but effective for the identification of the system. At last, the Bode diagram of the system is obtained as shown in the blue line in Fig. 11.

In order to simply the system, a second order transfer function is used to identify the system. The identified Bode diagram is shown in red line in Fig. 11, and the identified plant transfer function is as follows

$$G_n(s) = \frac{720}{(0.31s + 1)(0.001s + 1)} \tag{16}$$

As described in Section 3.2, nominal model of the plant is used to design DOB. The second order $Q(s)$ is selected. The choice of its parameters depends on the disturbance rejection ability by trial and error. An equivalent disturbance rejection rate is developed in this paper. As shown in Fig. 6, u_i is set as 0, and $d$is set as sinusoidal signal which has an amplitude of 0.86°and a frequency of 1Hz. We carried out lots of experiments with different parameters to verify the performance of DOB and determine the parameters of DOB. In particular, the typical comparison of the three experiments is shown in Fig. 12. It can be seen from Fig. 12, when DOB is added to the system, the peak of the gyro outputs with different methods are 87.36°/s without DOB, 19.18°/s with $\tau = 0.0045$, and 10.25°/s with $\tau = 0.0035$. Although, the disturbance rejection ability of the system is becoming better with the smaller value of τ, there occurs

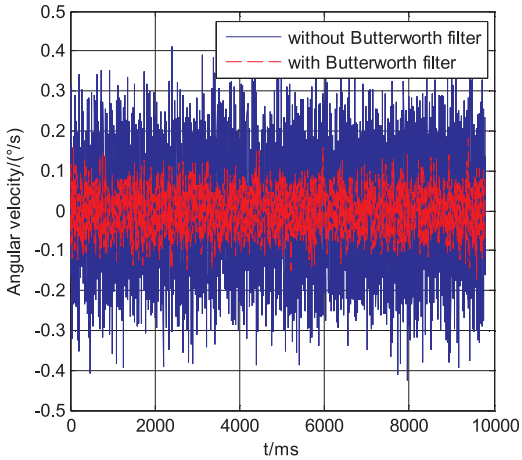

Fig. 10. Comparison of static output of gyro.

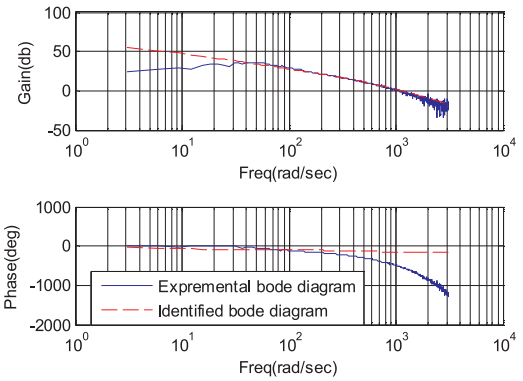

Fig. 11. Open loop Bode diagram and its identified Bode diagram for the stabilizing loop.

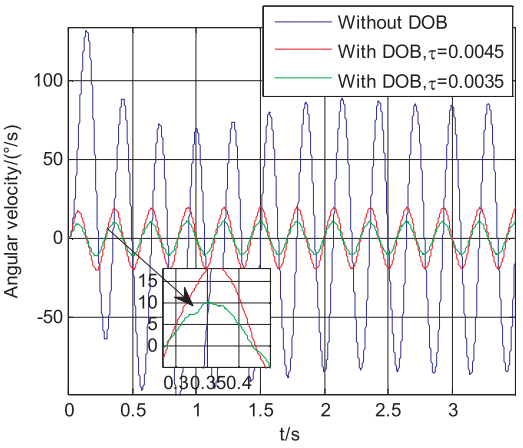

Fig. 12. Comparison of parameters of DOB.

deformation of the sinusoidal output of the system with the smaller value of τwhich is shown in amplified figure in Fig. 12. So we choose $\tau = 0.0045$in this paper.

Correlation analysis method is also used to identify the open loop system of stabilized loop with DOB. The range of random white noise is from -0.3 to 0.3. Then, the Bode diagram is shown in Fig. 13 in the blue line. It can be seen from the Fig. 13 that there is a point that has a peak value similarly to the resonance at 202.5 rad/s. If we do not deal with the point and design linear controller, this peak value will exist in the system that severely affects the performance of the system. So we need to eliminate the effect and the notch filter is intended to reach the aim (the evidence of this judgment can be seen from Fig. 16). According to the resonance point at 202.5 rad/s, we use the theory proposed in Section 3.3 to design the notch filter, where$A_{vf} = 1$ and $\omega_n = 202.5$. Then, we identify t open loop system of stabilized loop with DOB and notch filter by correlation analysis method. The Bode diagram is given in the red

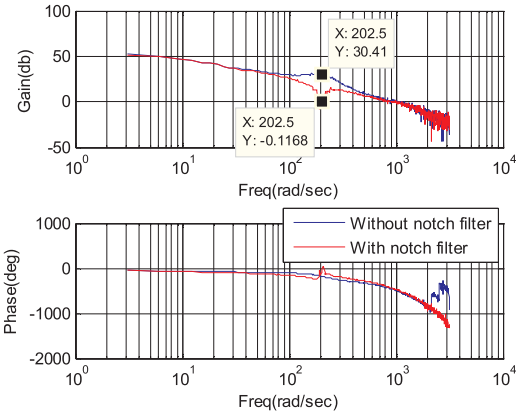

Fig. 13. Open loop Bode diagram for stabilizing loop with DOB.

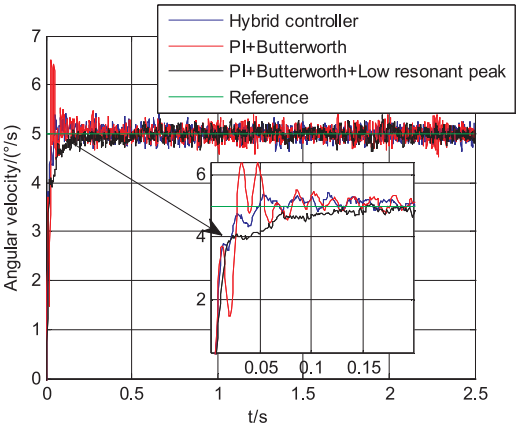

Fig. 14. Step response of closed loop system.

line in Fig. 13.

The next step is to design the IDPID. The four coefficients of IDPID controller are tuned by trial and error as follows: $k_p = 0.04$, $k_i = 0.2$, $k_d = 0.0003$, $N = 500$. Then, performance analysis is carried out in this paper. To compare the proposed controller strategy thoroughly, three controllers are considered. The parameters of traditional PI controller are as follows: $k_{pt} = 0.065$, $k_{it} = 2.0$ where $t$denotes traditional. In addition, all the compared controllers have the Butterworth filter inside. The step response and frequency characteristic are the performances to be verified on the stabilized platform.

Frequency analysis and time domain analysis are carried out. The results of the step response characteristics are shown in Fig. 14. It can be seen from Fig. 14 that the rise time of the system is 26 ms by two controllers (Hybrid controller and PI + Butterworth). However, the overshoot of the two responses by two controllers are different which is 0%, 30% respectively. The standard deviations of static error are 0.1072°/s, 0.1307°/s respectively. The frequency response of the system is shown in Fig. 15. Here, experimental sweep -frequency response data has taken from 0.9 Hz to 60 Hz in terms of the amplitude ratio and phase response. The experiments show that the bandwidth is 133.6 rad/s by hybrid controller. Although the bandwidth of traditional PI controller may be larger than the former, the resonant peak is 3.707 dB that is not allowed. Here, a lot of test has been done to improve the performance by the traditional PI controller, they are all vainly for this system, if the index of bandwidth is not reduced. As a result, a low bandwidth system is proposed to verify the whether the traditional PI controller can meet the demand. The parameters of traditional PI controller are set as $k_{ptl} = 0.040$, $k_{itl} = 0.2$denotes low bandwidth. The step response and frequency response are shown in black line in Fig. 14, and green line in Fig. 15 respectively. The result is that the overshoot is 0%, the rise time is 75 ms, and the standard deviation of static error is 0.1094°/s. Frequency response shows that the resonant peak value is reduced, but the bandwidth is 86.24 rad/s. Thus, the disadvantage of the traditional PI controller is distinctly, and traditional PI controller cannot meet the demand.

4.3. Performances verification on the seeker

P controller is used for tracking loop. The disturbance-rejecting rate and tracking performance of the seeker are the performances

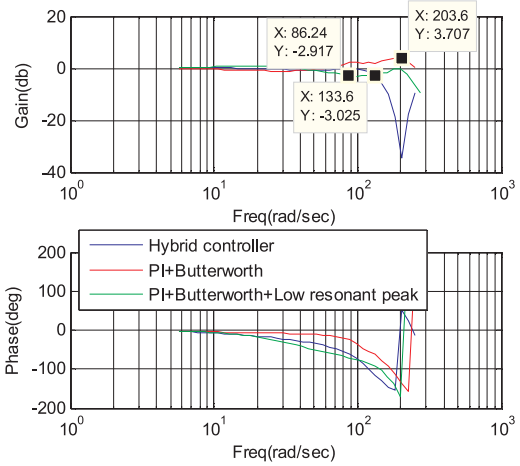

Fig. 15. Bode diagram of closed loop system.

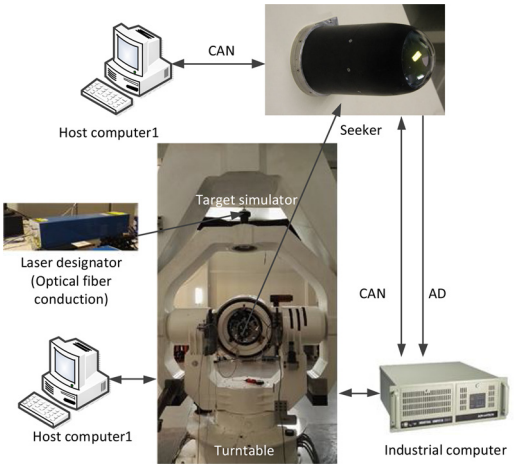

Fig. 16. Experimental setup of a seeker.

to be verified on the seeker that is mounted on the five-axis turntable shown in Fig. 16. The seeker is fitted on the three-axis turntable of five-axis turntable. Target simulator is fixed on the inner gimbal of the two-axis turntable. Laser designator radiate the lase by optical fiber conduction to the target simulator. In addition, the CAN communication is used in this experiment. Host computer 1 configures the programs and states to the seeker and monitors the states of the seeker. Host computer 2 configures the programs and states to the five-axis turntable. Industrial computer acquires the output of the sensors. The experiments of the hybrid controller and the PI + Butterworth + Low resonant peak are carried out in this section. The developed algorithm is implemented on the printed-circuit-board (PCB). A C language computer program is developed for control strategy by CCS5.5.

Tracking performance is tested by tracking trapezoid curve at 6°/s. The test process is as follows: the two-axis turntable that mounts with target simulator moves along the trapezoid signal; the seeker acquires the laser signal from target simulator and solves the laser code into LOS; the gimbals of the seeker equipped with the laser detector move to acquire, tracking, pointing the laser target. The moving data of the yaw gimbal is acquired and recorded by the industrial computer. The experimental result is shown in Fig. 17. It can be seen from the Fig. 17 that the response time is shorter using the proposed controller than using traditional controller. Of cause, the result is obvious, since the traditional PI controller has a lower bandwidth of stabilized loop.

Disturbance rejection ability is tested by tracking sinusoidal signal. When the three-axis turntable is posed a yaw axis disturbance with an amplitude of 1° and a frequency of 3.5 Hz. The target simulator on the two-axis turntable is static. Then, the moving data of the yaw gimbal of the platform is acquired and recorded by the industrial computer. The angular velocity is recorded and the disturbance rejection rate$J$is calculated by the traditional method shown in Eq. (17)

$$J = \frac{|\omega_{out}|}{|\omega_b|} \times 100\% \tag{17}$$

where $\omega_{out}$is the angular velocity of yaw axis, and $\omega_b$is the angular velocity of the three-axis turntable. The experimental result is shown in Fig. 18. It can be seen from Fig. 18 that the amplitudes of the gyro output are 1.2°/s and 0.3°/s. Because the amplitude of the input angular velocity is 12.25°/s, the disturbance rejection rate of the two controller are 2.45% and 9.8% respectively.

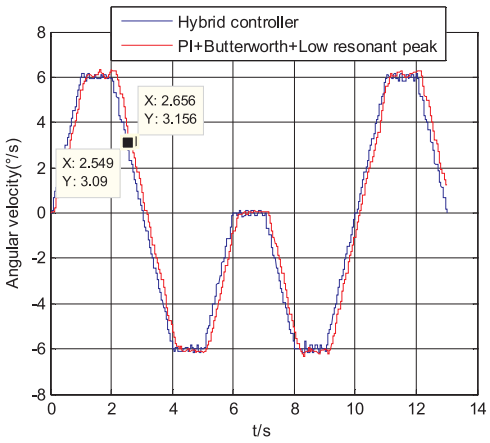

Fig. 17. Tracking performance of the seeker.

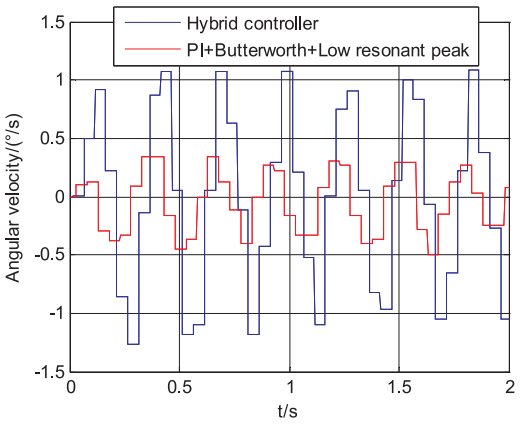

Fig. 18. Disturbance rejection rate of the seeker.

From above experiments, it can be concluded that in contrast to the traditional PI algorithm, the present procedure has the better performance. In particular, it not only improves the bandwidth but also the disturbance rejection rate. Static error has introduced the standard deviation to quantify the performance of the controller. The proposed method has relatively lower standard deviation, which illustrates the superiority of it.

5. Conclusions

The main contributions of this paper are: a hybrid controller is designed to the stabilized system; theoretically analysis is presented in the paper; validation of the method is done by experiments. The concept of hybrid controller including Butterworth low pass filter, DOB, notch filter and IDPID controller is discussed and detailed mathematical formulation for the design of the hybrid controller is presented. Butterworth low pass filter is used to attenuate the noise of the gyro. DOB is used to improve the disturbance rejection rate of the system. Notch filter is used to suppress the resonant frequency that is the obstacle to increase the bandwidth of the stabilized loop. IDPID controller is an excellent controller to balance the dynamics performance and noise of the system. In addition, the selection criteria of the controller parameters are given in the paper. Experiments are carried out on the stabilized platform and a certain seeker respectively to validate the effectiveness and practicability of the proposed strategy. The specifications of closed-loop like rise time, overshoot, bandwidth, disturbance rejection rate are all verified in the paper. According to the experiments, the proposed method obtains better design performance than traditional PI controller. The proposed strategy can eliminate the disturbance and obtain the best performance specification. Besides, the structure is concise and the parameters are easy to tune by the proposed selection criteria.

Author contributions

Mingyue Zhang conceived the methodology and wrote the paper. Hui Liu and Hongwei Zhang designed and performed the experiment. Xikui Miao checked the paper.

Conflicts of interest

The authors declare that there is no conflict of interests regarding the publication of this article.

Acknowledgments

We acknowledge Academic Editor for his careful revision of the language and grammatical structures in this article.

The author(s) disclosed receipt of the following financial support for the research, authorship, and/or publication of this article: The opening topic fund of Luoyang Electronic Equipment Test Center of China, Key Laboratory of Electro-Optical Countermeasures Test & Evaluation Technology (No. GKCP2017002). This support is gratefully acknowledged.

References

[1] Xing-long Li, Wen-jin Yao, Li-kun Zhu, Xiao-ming Wang, Ji-yan Yu, Ground target localization algorithm for semi-active laser terminal correction projectile, Def. Technol. 12 (3) (2016) 234–241.

[2] Peter J. Kennedy, Rhonda L. Kennedy, Direct versus indirect line of sight (LOS) stabilization, IEEE Trans. Control. Syst. Technol. 11 (1) (2003) 3–15.

[3] M. Řezáč, Z. Hurák, Structured MIMO H ∞ design for dual-stage inertial stabilization: case study for HIFOO and Hinfstruct solvers, Mechatronics 23 (8) (2013) 1084–1093.

[4] X. Zhou, H. Zhang, R. Yu, Decoupling control for two-axis inertially stabilized platform based on an inverse system and internal model control, Mechatronics 24

(8) (2014) 1203–1213.
[5] M.M. Abdo, A.R. Vali, A.R. Toloei, M.R. Arvan, Stabilization loop of a two axes gimbal system using self-tuning PID type fuzzy controller, ISA Trans. 53 (2) (2014) 591–602.
[6] S.L. Jianliang Mao, Li Qi, Jun Yang, Design and implementation of continuous finite-time sliding mode control for 2-DOF inertially stabilized platform subject to multiple disturbances, ISA Trans. (2018).
[7] J. Fang, R. Yin, X. Lei, An adaptive decoupling control for three-axis gyro stabilized platform based on neural networks, Mechatronics 27 (2015) 38–46.
[8] Z.Z. Changrui Bai, A least mean square based active disturbance rejection control for an inertially stabilized platform, Optik 174 (2018) 609–622.
[9] S. Li, C. Wu, Z. Sun, Design and implementation of clutch control for automotive transmissions using terminal sliding mode control and uncertainty observer, IEEE Trans. Veh. Technol. 65 (4) (2016) 1890–1898.
[10] J.Y. Jianliang Mao, Shihua Li, Li. Qi, Output feedback stabilization of inertial stabilized platform with unmatched disturbances using sliding mode approach, IFAC-PapersOnLine. 50 (1) (2017) 5149–5154.
[11] J. Han, From PID to active disturbance rejection control, IEEE Trans. Ind. Electron. 56 (3) (2009) 900–906.
[12] J. Yang, S. Li, J. Su, X. Yu, Continuous nonsingular terminal sliding mode control for systems with mismatched disturbances, Automatica. 49 (7) (2013) 2287–2291.
[13] K. Ohishi, M. Nakao, K. Ohnishi, K. Miyachi, Microprocessor-controlled DC motor for load-insensitive position servo system, IEEE Trans. Ind. Electron. 34 (1) (1987) 44–49.
[14] W.H. Chen, J. Yang, L. Guo, S. Li, Disturbance observer-based control and related methods: an overview, IEEE Trans. Ind. Electron. 63 (2) (2016) 1083–1095.
[15] C.J. Kempf, S. Kobayashi, Disturbance observer and feedforward design for a high-speed direct-drive positioning table, IEEE Trans. Control Systems Technol. 7 (5) (1999) 513–526.
[16] X. Zhou, J. Yuan, Z. Qiang, T. Cai, Dual-rate-loop control based on disturbance observer of angular acceleration for a three-axis aerial inertially stabilized platform, ISA Trans. 63 (2016) 288–298.
[17] L.I. Jia-Quan, C. Ding, D.J. Kong, C.L. Yin, M. Dai, Velocity based disturbance observer and its application to photoelectric stabilized platform, Opt. Precis. Eng. 19 (5) (2011) 998–1004.
[18] F. Königseder, W. Kemmetmüller, A. Kugi, Attitude control strategy for a camera stabilization platform, Mechatronics 46 (2017) 60–69.
[19] D.G.E. Robertson, J.J. Dowling, Design and responses of Butterworth and critically damped digital filters, J. Electromyogr. Kinesiol. 13 (6) (2003) 569–573.
[20] D.A. Winter, Biomechanics and Motor Control of Human Movement, Wiley, New York, 1990.
[21] H.S. Lee, Robust Digital Tracking Controllers for High Speed/High Accurancy Positioning Systems, MechEngDep, UnivCaliformia, Berkeley, 1994 Ph.D dissertation.
[22] J. Li, X. Qi, L. Feng, Correlation analysis method based SISO neuro-fuzzy Wiener model, J. Process Control 58 (2017) 73–89.
[23] M.S. Ahmed, Estimation of difference equation parameters of SISO systems by correlation analysis, Int. J. Control 35 (4) (1982) 677–687.
[24] J.D. Hill, G.J. Mcmurtry, An application of digital computers to linear system identification, IEEE Trans. Automat. Contr. 9 (4) (1964) 536–538.